

FAST observations of VLF waves in the auroral zone: Evidence of very low plasma densities

R. J. Strangeway,¹ L. Kepko,¹ R. C. Elphic,² C. W. Carlson,³ R. E. Ergun,³
J. P. McFadden,³ W. J. Peria,³ G. T. Delory,³ C. C. Chaston,³ M. Temerin,³
C. A. Cattell,⁴ E. Möbius,⁵ L. M. Kistler,⁵ D. M. Klumpar,⁶
W. K. Peterson,⁶ E. G. Shelley,⁶ and R. F. Pfaff,⁷

Abstract. The Fast Auroral SnapshoT (FAST) explorer frequently observes the auroral density cavity, which is the source region for Auroral Kilometric Radiation (AKR). An important factor in the generation of AKR is the relative abundance of hot and cold electrons within the cavity, since hot electrons introduce relativistic modifications to the wave dispersion. VLF wave-form data acquired by FAST within the auroral density cavity show clear signatures of whistler-mode waves propagating on the resonance cone. This allows us to obtain the electron plasma frequency, and the cavity often has densities $< 1 \text{ cm}^{-3}$. Moreover, the hot electrons can be the dominant electron species, enabling AKR to be generated below the cold electron gyro-frequency.

Introduction

It has long been known that there is a deep density cavity at high altitudes on auroral zone field lines [Calvert, 1981]. Such a cavity is necessary for the generation of Auroral Kilometric Radiation (AKR) by the cyclotron maser instability [Wu and Lee, 1979]. Simulations [Pritchett and Strangeway, 1985] have shown that gradients in the primary auroral electron distribution, rather than the upgoing loss-cone, can be the source of AKR if the hot electrons dominate the wave dispersion so that the R–X mode cut-off lies below the cold electron gyro-frequency. Data from the Fast Auroral SnapshoT (FAST) explorer support the primary auroral electrons as being the source of AKR [Delory *et al.*, 1998]. Alternatively, on the basis of Viking observations of low densities in the auroral cavity [Perraut *et al.*, 1990; Hilgers *et al.*, 1992], Roux *et al.* [1993] argue that AKR is generated by electrons trapped by time-varying electric fields. In either case relativistic modifications to the wave dispersion are necessary. Determining if such effects are present requires knowledge of the relative abundance of hot and cold electrons.

Measuring electron number density is difficult, especially at low energies, where spacecraft photoelectrons often dominate the electron flux. In this paper we present data acquired by FAST in the auroral density cavity, and we show that VLF waves propagating on the whistler-mode resonance cone provide a means for determining the electron density. We find that at times the hot electrons are the dominant species, and relativistic modifications to the wave dispersion are an essential component in the generation of AKR.

Example of a Density Cavity: Orbit 1761

Figure 1 summarizes the FAST particles and fields data for the auroral density cavity observed on orbit 1761 near 22 MLT. Figure 1a shows electric field data in the frequency range 300–800 kHz. The white trace is the electron gyro-frequency calculated from the magnetometer observations. Near the center interval the wave frequency drops to or even slightly below the electron gyro-frequency. This is a strong indication that we are in the local AKR source region.

Figure 1b shows VLF spectra generated through on-board Fast Fourier Transforms (FFTs). The white trace gives the proton gyro-frequency. The VLF data show clear spin modulation, which we will discuss further below.

Figure 1c shows the electron energy spectra, integrated over all pitch angles, while Figure 1d shows pitch-angle spectra integrated over energies $> 20 \text{ eV}$. Figures 1e and 1f show the ion energy and pitch-angle spectra, with the pitch-angle spectra integrated over energies $> 4 \text{ eV}$. A pitch-angle of 180° corresponds to upgoing particles. The particle spectra show many of the characteristics of acceleration through a parallel electric field. From 06:43:48 to 06:44:45 UT the ion and electron spectra are relatively mono-energetic, and the ions are narrowly confined to a few degrees around 180° pitch angle, indicating that the electric field structure extends both above and below the FAST spacecraft. From 06:44:45 to 06:44:58 the potential moves almost entirely above the spacecraft, with the ions showing a conic-like structure and lower energy electrons appearing within the upgoing source cone. After this time the ions become more beam-like, and the lower energy electrons are absent, consistent with the potential extending to lower altitudes.

Figure 1g gives the deviation of the observed magnetic field from the model field (IGRF 95 with secular variation) in field-aligned coordinates: outwards (o), eastwards (e), and model-field aligned (b). FAST is moving to higher latitudes in the northern hemisphere, and the negative deflection in the eastward component marks an upward field-aligned current, as expected in a region of precipitating electrons.

¹Institute of Geophysics and Planetary Physics, University of California, Los Angeles.

²Los Alamos National Laboratory, Los Alamos, New Mexico.

³Space Sciences Laboratory, University of California, Berkeley.

⁴University of Minnesota, Minneapolis.

⁵University of New Hampshire, Durham.

⁶Lockheed Martin Palo Alto Research Laboratory, Palo Alto, California.

⁷NASA Goddard Space Flight Center, Greenbelt, Maryland.

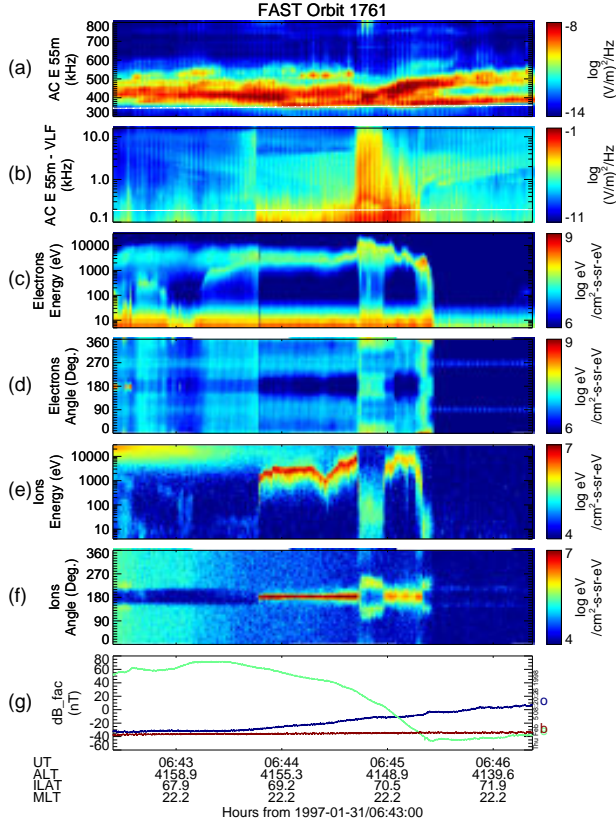


Figure 1. Particles and fields data acquired by FAST in the auroral density cavity.

The parallel electric field will reduce the plasma density, but it is difficult to calculate total density from the particle spectra because of contamination by photoelectrons. Instead, we can use the VLF wave data to provide quantitative estimates of the plasma density. Figure 2 shows FFTs of the 16 kHz Nyquist frequency burst mode data (32,768 samples per second) from (a) the 55m electric field antenna and (b) the 21''-core search coil sensor. For increasing frequency the superimposed traces show the proton gyro-frequency (blue), the lower hybrid resonance frequency (green), and the electron plasma frequency (yellow). The latter two frequencies are determined through fits to the whistler-mode dispersion relation, as we discuss later. Both sensors lie in or near the spacecraft spin plane. FAST has a spin period ≈ 5 s, and is oriented such that the ambient magnetic field lies close to the spin plane. The VLF data show clear modulation at twice the spin frequency. Therefore, the signals are polarized with the minimum in wave power occurring when the antenna is perpendicular to the wave field. Prior to 06:44:43 UT the phase of the electric field spin modulation is clearly frequency dependent. Unlike the magnetic field, the electric field minima are curved as a function of frequency, with the minima at ~ 4 kHz occurring 1/4 spin period earlier than at ~ 200 Hz. *Temerin* [1984] reported similar observations from the S3-3 spacecraft. The signature shown in Figure 2 is characteristic of whistler-mode waves propagating on the resonance cone.

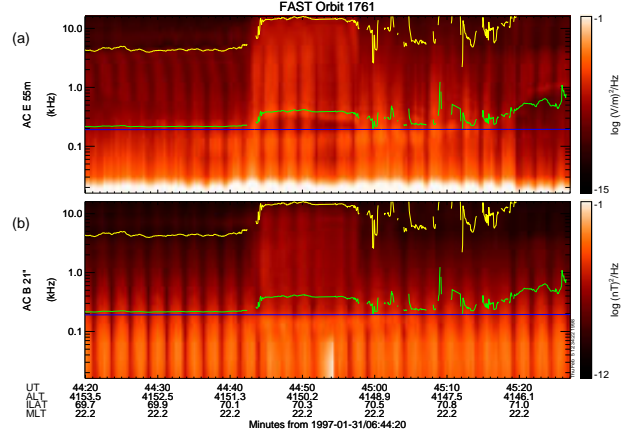


Figure 2. Fast Fourier Transforms of 16 kHz Nyquist frequency burst-mode data.

VLF Wave Modes in a Low Density Plasma

The electron plasma frequency (ω_{pe}) is usually much less than the electron gyro-frequency (Ω_e) in the auroral density cavity. The two superluminal (faster than light) modes in the VLF range are the L-O and L-X modes. The L-O mode propagates for $\omega \geq \omega_{pe}$, while the L-X mode lies in the range $\omega_{LX} \leq \omega \leq \omega_{pe}$. When $\omega_{pe} \ll \Omega_e$,

$$\omega_{LX} \approx \Omega_i + \omega_{pe}^2 / \Omega_e \approx \Omega_i (1 + \omega_{pi}^2 / \Omega_i^2) \quad (1)$$

where ω_{pi} is the ion plasma frequency, and Ω_i is the ion gyro-frequency, assuming only one ion species. Above ω_{pe} the L-X mode couples into the subluminal Z-mode.

For a cold plasma the two subluminal modes with $\omega < \omega_{pe}$ are the whistler mode and, for $\omega < \Omega_i$, the shear Alfvén mode. At large wave number the whistler mode is quasi-electrostatic and propagates at the resonance cone angle (θ_r) with respect to the ambient field. From the quasi-transverse

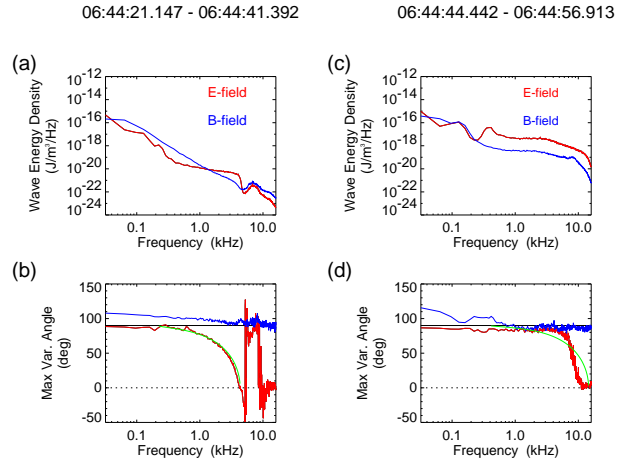


Figure 3. Maximum variance analysis for selected intervals of data as shown in Figure 2.

approximation to the Appleton-Hartree dispersion relation

$$\cos^2 \theta_r \approx (\omega^2 - \omega_{\text{LHR}}^2) / \omega_{\text{pe}}^2 \quad (2)$$

where ω_{LHR} is the lower hybrid resonance frequency, and

$$\omega_{\text{LHR}} \approx \Omega_i (1 + \omega_{\text{pi}}^2 / \Omega_i^2)^{1/2} \quad (3)$$

since $\omega_{\text{pe}} \ll \Omega_e$. The electric field of a wave on the resonance cone is polarized such that $E_{\parallel} / E_{\perp} \approx \cot \theta_r$, where \parallel and \perp are defined with respect to the ambient magnetic field.

The first of two approaches we employ to analyze the VLF waves uses data from a single spinning sensor to determine the spin-phase angle that maximizes the variance of the wave electric field (θ_v). Each frequency component of sequential FFTs of the spinning data (e.g., Figure 2) is treated as a separate time series. We then determine θ_v for each frequency, in a manner analogous to linear least squares regression. The main differences are that the fit line maximizes the variance along the fit line itself, and that this line passes through the origin. This method requires an integral number of spins of data, and the data should be similar from spin to spin, as occurs for example in the first third of Figure 2. Having obtained θ_v for different frequencies, we fit $\cos \theta_v$ to the right-hand side of (2) to deduce ω_{pe} . Prior to performing the fits, we restrict the data to that portion where $\cos \theta_v$ varies approximately linearly with frequency. We minimize the absolute deviation rather than the variance in determining the fit, since the resultant fit is less affected by outliers.

Neither of the requirements for the maximum variance method applies to our second approach, which uses despun data (see also *Ergun et al.* [1998]). FFTs of the despun electric field data are fit to (2), assuming $E_{\parallel} / E_{\perp} = \cot \theta_r$. We take FFTs five at a time to increase the density of points for the fit, and again minimize the absolute deviation to determine the fit. In obtaining the fit, the wave data are restricted to $\omega_{\text{LHR}} < \omega < \omega_{\text{pe}}$. This restriction is applied iteratively until the inferred plasma frequency does not change. A 90% significance chi-square goodness-of-fit test is then applied. The electron plasma frequency and lower hybrid resonance frequency shown in Figure 2 were determined by this method. Many of the fits to the data in the latter portion of Figure 2 failed the chi-square test and were eliminated.

It is useful to compare the two methods. Figure 3a shows the energy densities of the electric (red) and magnetic (blue) fields, using data from the first part of Figure 2 where the spectra show a clear cut-off near 4 kHz. The electric and magnetic energy densities are equal for a purely transverse wave propagating at the speed of light. The magnetic field spectrum is at background, apart from some waves above 4 kHz. We do not know at this time if the background noise is either intrinsic to the instrument or from an external source. Above the 4 kHz transition, Z-mode and possibly L-O mode waves may be present, although the waves appear to have phase velocities less than the speed of light.

Figure 3b shows the maximum variance phase angle of both the electric and magnetic fields for the same interval as in Figure 3a. The green trace shows the expected phase angle from (2) using the median values of the plasma frequency and lower hybrid frequency for the interval, obtained by fitting despun wave spectra to (2). The comparison provides a useful consistency check; the overlap of the two curves is strong evidence that the waves are on the whistler-mode res-

onance cone. The plasma frequency is hence about 4 kHz, and the total electron number density (n_t) is $\approx 0.25 \text{ cm}^{-3}$.

In Figures 3c and 3d data from the central interval of Figure 2 are used and both electric and magnetic field spectra are well above background for most frequencies. Above 300 Hz the implied phase velocity is about three times the speed of light, and the waves could be either superluminal L-X mode or quasi-electrostatic whistler mode. In addition, Figure 3d shows some discrepancy between the whistler-mode fit of the despun data and the maximum variance analysis. From the fit, the electron plasma frequency $\approx 12 \text{ kHz}$, and $\omega_{\text{LHR}} \approx 1.7\Omega_i$. If we interpret the waves as L-X mode waves, then the plasma frequency $\approx 8 \text{ kHz}$, and $\omega_{\text{LX}} \approx 2\Omega_i$. Thus both wave modes give a similar lower frequency cut-off. There is some ambiguity in mode identification for this interval, with the whistler-mode fit giving a higher plasma frequency than we would infer for the L-X mode.

Statistical Survey of the Deep Auroral Cavity

FAST passed through the nightside auroral oval in the 22 to 24 MLT range on orbits 1740–1779, and we used data from these orbits for our statistical survey. There was some preselection of the data. First, 16 kHz Nyquist frequency burst-mode data had to be available. Second, we restricted our analysis to intervals where there was a strong field-aligned ion beam and a deep minimum in the electron energy flux spectra, indicating that the spacecraft was in the acceleration region. Thus, for example, only the first third of the interval in Figure 2 was included in our statistics. The central portion was excluded since the spacecraft was below the acceleration region. Third, the spacecraft data rate had to be constant throughout the interval of interest. These selection criteria left 28 cavities from the original 40 orbits.

Figure 4 shows the results of this analysis. Figure 4a gives the electron plasma frequency (f_{pe}) for each cavity calculated from fits to (2) of either despun electric field data (open circles), in which case the median value is used, or the maximum variance phase angle (closed circles). The symbols are connected when plasma frequency estimates from both methods are available. The data are plotted as a function of the median characteristic electron energy, which is given by the ratio of the energy flux to number flux for energies $> 100 \text{ eV}$. For many of the cavities $f_{\text{pe}} < 9 \text{ kHz}$ ($n_t < 1 \text{ cm}^{-3}$).

Figure 4b gives the ratio of hot to total electron number density (n_h / n_t), where n_h is calculated from the observed fluxes for energies $> 100 \text{ eV}$. There is an indication that the density ratio is higher for lower energy. Figure 1 shows that both the electron energy and the flux of secondaries increases when the potential moves above the spacecraft, possibly explaining the trend in Figure 4b. Figure 4c, however, shows that the ion beam energy also increases with the electron energy, and the increase in electron energy is associated with an increase in the total potential, not movement of the accelerating potential. The trend in Figure 4b may have implications for the generation of AKR. As the electron energy increases the relativistic correction to the hot electron gyro-frequency increases. The proportion of low energy electrons can also increase yet still allow the R-X mode cut-off to lie below the cold electron gyro-frequency. High frequency wave-form data indicate that the R-X mode cut-off can lie below the electron gyro-frequency [*Ergun et al.*, 1998].

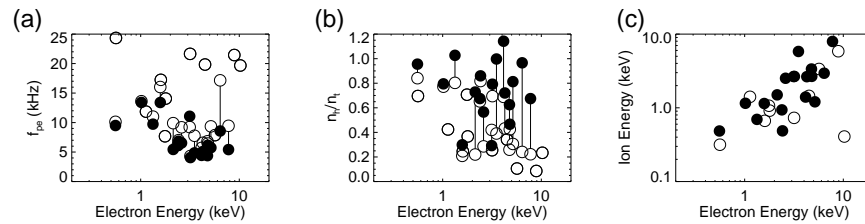


Figure 4. Inferred plasma frequency and electron density ratio for 28 auroral density cavities. Also shown is the median ion beam energy for each cavity.

Conclusions

VLF data acquired in the auroral density cavity by FAST show clear evidence of whistler-mode waves propagating on the resonance cone. This allows us to determine the electron plasma frequency. A survey of 28 density cavities finds that the electron density is often less than 1 cm^{-3} . Furthermore, the hot electron density can be comparable to the inferred total density. Since we have used a cold plasma dispersion analysis, the density could be lower, and it is possible that there are no cold electrons within the cavity. Hot electrons will modify the wave dispersion near the electron gyro-frequency [Pritchett, 1984], but a significant cold electron population could decouple the unstable mode from the R-X mode [Strangeway, 1985; 1986]. Clearly, future wave dispersion analysis should assess relativistic modifications using distribution functions that retain as many of the features of the observed distributions as possible.

The FAST observations may also have consequences for mechanisms to maintain the parallel electric field on auroral zone field lines. Koskinen *et al.* [1990] argue that low energy electrons are necessary to maintain what are referred to as weak double layers. More data would strengthen this conclusion, but it appears that such double layers cannot be responsible for the net potential in the auroral acceleration region. Our results are a strong indication that cold electrons are almost completely evacuated from this region.

References

- Calvert, W., The auroral plasma cavity, *Geophys. Res. Lett.*, *8*, 919-921, 1981.
- Delory, G. T., et al., FAST observations of electron distributions within AKR source regions, *Geophys. Res. Lett.*, in press, 1998.
- Ergun, R. E., et al., FAST satellite observations in the AKR source region, *Geophys. Res. Lett.*, in press, 1998.
- Hilgers, A., B. Holback, G. Holmgren, and R. Boström, Probe measurements of low plasma densities with applications to the auroral acceleration region and auroral kilometric radiation sources, *J. Geophys. Res.*, *97*, 8631-8641, 1992.
- Koskinen, H. E. J., R. Lundin, and B. Holback, On the plasma environment of solitary waves and weak double layers, *J. Geophys. Res.*, *95*, 5921-5929, 1990.
- Perraut, S., et al., Density measurements in key regions of the Earth's magnetosphere: Cusp and auroral region, *J. Geophys. Res.*, *95*, 5997-6014, 1990.
- Pritchett, P. L., Relativistic dispersion, the cyclotron maser instability, and auroral kilometric radiation, *J. Geophys. Res.*, *89*, 8957-8970, 1984.
- Pritchett, P. L., and R. J. Strangeway, A simulation study of kilometric radiation generation along an auroral field line, *J. Geophys. Res.*, *90*, 9650-9662, 1985.
- Roux, A., et al., Auroral kilometric radiation sources: In situ and remote observations from Viking, *J. Geophys. Res.*, *98*, 11,657-11,670, 1993.
- Strangeway, R. J., Wave dispersion and ray propagation in a weakly relativistic electron plasma: implications for the generation of auroral kilometric radiation, *J. Geophys. Res.*, *90*, 9675-9687, 1985.
- Strangeway, R. J., On the applicability of relativistic dispersion to auroral zone electron distributions, *J. Geophys. Res.*, *91*, 3152-3166, 1986.
- Temerin, M., Electron density and whistler mode propagation characteristics at 7000 km altitude in the auroral zone and polar cap, *J. Geophys. Res.*, *89*, 3945-3950, 1984.
- Wu, C. S., and L. C. Lee, A theory of terrestrial kilometric radiation, *Astrophys. J.*, *230*, 621-626, 1979.
- L. Kepko and R. J. Strangeway, Institute of Geophysics and Planetary Physics, University of California at Los Angeles, 405 Hilgard Ave., Los Angeles, CA 90095. (e-mail: strange@igpp.ucla.edu)
- R. C. Elphic, Space and Atmospheric Sciences, MS D466, Los Alamos National Laboratory, Los Alamos, NM 87545.
- C. W. Carlson, C. C. Chaston, G. T. Delory, R. E. Ergun, J. P. McFadden, W. J. Peria, and M. Temerin, Space Sciences Laboratory, University of California, Berkeley, CA 94720.
- C. A. Cattell, School of Physics and Astronomy, University of Minnesota, 116 Church St., S.E., Minneapolis, MN 55455.
- L. M. Kistler, E. Möbius, Dept. of Physics and Inst. for the Study of Earth, Oceans and Space, University of New Hampshire, Durham, NH 03824
- D. M. Klumpar, W. K. Peterson, E. G. Shelley, Lockheed Martin Palo Alto Research Laboratory, 3251 Hanover St., Palo Alto, CA 94304.
- R. F. Pfaff, Code 696, NASA Goddard Space Flight Center, Greenbelt, MD 20771.

(Received December 17, 1997; revised February 6, 1998; accepted February 10, 1998.)